Impulse approximation for cusp electron production from target K and L shells

D. H. Jakubassa-Amundsen
Sektion Physik, Universität München, D-8046 Garching bei München, West Germany
(Received 17 December 1987)

The forward peak resulting from electron capture to the continuum of bare projectiles is investigated within the impulse approximation in both its prior and post form. It is found that the asymmetry of the peak as well as the peak intensity increases if a larger number of interactions between the electron and the projectile is included in the calculation. For strongly asymmetric systems with light projectiles, a peaking approximation becomes valid which factorizes the capture cross section into the ionization cross section times the projectile Coulomb normalization. Thus capture from excited states is easily included, and the factorization allows for a fast evaluation not only of the electron spectra but also of the impact-parameter distribution and the alignment. The theory is also extended to capture into Rydberg states. The collision systems $He^{2+}+He$, $p+He$, and $p+Ne$ are investigated, and comparison is made with available experimental data.

I. INTRODUCTION

The investigation of the forward peak in fast-ion–atom collisions has attracted great interest lately both experimentally and theoretically.[1] For bare projectiles, the forward peak consists of target electrons which are ejected with the same velocity as the projectile and which thus are captured into low-lying projectile continuum states. At the exact velocity matching, the doubly differential capture cross section is mathematically divergent (which gives rise to the name "cusp") and in addition has a step discontinuity, leading to a strong enhancement of electron emission on the low-energy side of the peak. This feature emerges from a numerical integration of the Schrödinger equation,[2] and is also present in the second-order Born approximation[3,4] or in other high-order theories,[5] such as the impulse approximation[6] (IA) and the continuum distorted-wave (CDW) approximation.[7] However, as far as the prediction of the magnitude of the peak skewness is concerned, the theories differ greatly from each other.

Experimental information is veiled by the fact that the detector resolution has a decisive influence on the peak shape. However, an expansion of the doubly differential cross section in terms of the electron velocity and emission angle in the projectile reference frame (with expansion coefficients B_{nl}), convoluted with the detector resolution, has made possible a systematic extraction of B_{nl} from experimental spectra by means of a fitting procedure.[8–13] Together with the fact that the cross sections can now be measured even on an absolute scale,[9,11,12,14] this allows for a detailed comparison between experiment and theory. The dipole asymmetry parameter $\beta=B_{01}/B_{00}$ with its strong dependence on projectile charge and collision velocity is especially suited for the test of capture theories, because due to the vanishing of β in a first-order theory, it makes higher-order effects directly accessible.

Up to now systematic investigations have only been carried out in a high-energy approximation of the second-order Born theory[7,15] and in the CDW approximation.[7] While the peaked second Born theory fails completely, the CDW scheme compares well with experimental data as far as absolute capture cross sections are concerned, but underestimates the peak skewness.

This matter of fact calls for the investigation of another capture theory, the impulse approximation.[16,17] In contrast to the second Born or CDW theory, which are symmetric in both electron-nucleus potentials, the IA is an asymmetric theory, including one of the potentials to all orders in the on-shell approximation, while being a first-order theory in the other field. Off-shell effects can safely be neglected near the ionization threshold of the projectile, as has been shown in the case of radiative capture.[18] The post-prior discrepancy of the impulse approximation for near-symmetric systems is one subject of this work: the prior IA for the capture into the continuum (CTC) is developed in Sec. II A within three different peaking approximations, while the post IA is briefly reviewed in Sec. II B. An extraction of the parameters B_{00} and β from the calculations and a comparison with experiment and with other theories for p and He^{2+} on He is performed in Sec. III A.

For systems with much heavier targets, capture from higher shells comes into play. L-shell CTC has first been measured by Sarkadi *et al.*,[19] but is also inherent in other CTC measurements at lower collision velocities.[20] In such strongly asymmetric systems, the prior IA has to be used: in Sec. III B it is applied to the calculation of K- and L-shell CTC in $p+Ne$ collisions, and the sum spectrum is compared to new experimental data. The impact-parameter dependence and the L-subshell alignment is also investigated (Sec. III C).

The theory of capture to the continuum is easily reformulated for the case of capture into Rydberg states of the projectile. The continuity of the capture amplitudes across the ionization threshold[21] allows for a relation between the B_{nl} and expectation values of the bound-state statistical multipoles[22] in the limit of high main quantum numbers, $n\to\infty$. This relation has been proved numeri-

cally for B_{00} and β within the CDW theory[22,23] and demonstrates that bound-state calculations may be used as substitute for the more complicated CTC calculations. In Sec. IV the peaked prior IA is used to investigate the continuity relation, and also the question to which extent the target electrons are not captured into the continuum, but into Rydberg states. A short conclusion follows (Sec. V). Atomic units ($\hbar=m=e=1$) are used unless otherwise indicated.

II. THEORY

Let us restrict ourselves to the independent-electron approximation, where only the target electron which is transferred to the bare projectile is considered. The other target electrons may be incorporated into an effective potential. Simultaneous excitation of the target will then also be neglected. For the description of the capture cross section, the impulse approximation is used. We give formulas for its prior form, which becomes the more accurate, the smaller the projectile charge Z_P as compared with the target charge Z_T, and address also the post form (for $Z_P \geq Z_T$).

A. Impulse approximation in the prior form

In the semiclassical theory where the internuclear coordinate $\mathbf{R}$ is approximated by a time-dependent trajectory with impact parameter $\mathbf{b}$, the transition amplitude for electron capture by light projectiles is given by[17]

$$a_{fi}^{\text{prior}} = -i\int_{-\infty}^{\infty} dt \int d\mathbf{q}\, \langle \psi_f^P \mid \mathbf{q}\rangle \langle \psi_{\mathbf{q}}^T \mid V_P \mid \psi_i^T\rangle \ , \tag{2.1}$$

describing the electron transfer in terms of excitation from the initial state ψ_i^T via the projectile field V_P into a continuum target state $\psi_{\mathbf{q}}^T$ with momentum $\mathbf{q}$. This is weighted with the momentum distribution of the final projectile state ψ_f^P, which has been transformed into the target frame of reference. $|\mathbf{q}\rangle$ denotes an electronic plane wave. Introducing the Fourier representation of the Coulomb field V_P, one has

$$a_{fi}^{\text{prior}} = \frac{iZ_P}{2\pi^2}\int_{-\infty}^{\infty} dt \int d\mathbf{q}\, e^{i(\kappa_f^2/2-\varepsilon_i^T+v^2/2)t} e^{i(\mathbf{q}-\mathbf{v})\mathbf{R}} \varphi_{\boldsymbol{\kappa}_f}^{*P}(\mathbf{q}-\mathbf{v}) \int d\mathbf{s}\frac{1}{s^2} e^{-i\mathbf{s}\cdot\mathbf{R}} \langle \psi_{\mathbf{q}}^T(\mathbf{r}) \mid e^{i\mathbf{s}\cdot\mathbf{r}} \mid \psi_i^T(\mathbf{r})\rangle \ . \tag{2.2}$$

In this expression, $\mathbf{v}$ is the collision velocity, $\varphi_{\boldsymbol{\kappa}_f}^P$ is the Fourier transformed continuum projectile state, and ε_i^T and $\kappa_f^2/2$ is the electronic energy in its initial and final state, respectively. The time integral is easily carried out in the case of a straight-line trajectory, and by transforming the coordinates $\mathbf{q}$ and $\mathbf{s}$ into $\mathbf{q}_1=\mathbf{q}-\mathbf{v}-\mathbf{s}$ and $\mathbf{s}_1=\mathbf{q}_1+\mathbf{s}-\boldsymbol{\kappa}_f$, respectively, one obtains

$$a_{fi}^{\text{prior}} = \frac{iZ_P}{\pi}\int d\mathbf{q}_1\, e^{i\mathbf{q}_1\cdot\mathbf{b}} \delta(\kappa_f^2/2-\varepsilon_i^T+\mathbf{q}_1\mathbf{v}+v^2/2) M(\mathbf{q}_1) \ ,$$

$$M(\mathbf{q}_1) = \int d\mathbf{s}_1 \frac{1}{(\mathbf{s}_1-\mathbf{q}_1+\boldsymbol{\kappa}_f)^2} \varphi_{\boldsymbol{\kappa}_f}^{*P}(\mathbf{s}_1+\boldsymbol{\kappa}_f) \times \langle \psi_{\mathbf{s}_1+\mathbf{k}_f}^T(\mathbf{r}) \mid e^{i(\mathbf{s}_1-\mathbf{q}_1+\boldsymbol{\kappa}_f)\cdot\mathbf{r}} \mid \psi_i^T(\mathbf{r})\rangle \ . \tag{2.3}$$

Upon squaring and integrating over the impact parameter, the doubly differential cross section for the emission of electrons with energy $E_f=k_f^2/2$ (where $\mathbf{k}_f=\boldsymbol{\kappa}_f+\mathbf{v}$) into the solid angle $d\Omega_f$ in the target frame of reference emerges,

$$\frac{d^2\sigma^{\text{prior}}}{dE_f\, d\Omega_f} = \frac{4Z_P^2 k_f}{v^2} N_i \int_{q_{\min}}^{\infty} dq_1\, q_1 \int_0^{2\pi} d\varphi_{q_1} \mid M(\mathbf{q}_1)\mid^2 \ ,$$

$$q_{\min} = \frac{1}{v}(\kappa_f^2/2-\varepsilon_i^T+v^2/2) \ , \tag{2.4}$$

where spherical coordinates have been used and the angle $\cos\vartheta_{q_1} = -q_{\min}/q_1$ is determined by the δ function. N_i is the number of electrons in the initial state.

Since $M(\mathbf{q}_1)$ implies a three-dimensional integral, an exact evaluation of (2.4) hardly seems possible, especially because the integrand is strongly oscillating in the region of $\kappa_f \approx 0$, due to the behavior of the Fourier-transformed Coulomb wave. We shall therefore perform the evaluation by means of a peaking approximation, which is based on the fact that $\varphi_{\boldsymbol{\kappa}_f}^P(\mathbf{s}_1+\boldsymbol{\kappa}_f)$ is strongly peaked at $\mathbf{s}_1=0$. Such an approximation is all the more justified, the higher the collision velocity ($v \gg Z_P$) and the larger the asymmetry ($Z_P \ll Z_T$), which is to be compared with the criteria of validity of the IA itself ($Z_P \ll Z_T$ and $v \gtrsim Z_T$ or $Z_P \lesssim Z_T$ and $v \gg Z_P$).

The simplest of successively less restrictive approximations, the so-called full peaking (FP) approximation,[17] reduces $M(\mathbf{q}_1)$ to an analytical expression by taking everything but $\varphi_{\boldsymbol{\kappa}_f}^P$ outside the integral at $\mathbf{s}_1=0$. The remaining integration then yields $(2\pi)^{3/2}$ times the coordinate space wave function at the origin, $\psi_{\boldsymbol{\kappa}_f}^P(\mathbf{r}=0)$.

If, in addition to $\varphi_{\boldsymbol{\kappa}_f}^P$, the Fourier transform of the potential, $(\mathbf{s}_1-\mathbf{q}_1+\boldsymbol{\kappa}_f)^{-2}$ is kept inside the integral, $M(\mathbf{q}_1)$ can still be evaluated analytically for a Coulomb wave function

$$M^{\text{FP2}}(\mathbf{q}_1) = e^{\pi\eta_f/2}\Gamma(1-i\eta_f)\frac{1}{(\mathbf{q}_1-\boldsymbol{\kappa}_f)^2} \times \left[\frac{q_1^2-(\kappa_f+i\varepsilon)^2}{(\mathbf{q}_1-\boldsymbol{\kappa}_f)^2}\right]^{-i\eta_f} \times \langle \psi_{\mathbf{k}_f}^T(\mathbf{r}) \mid e^{i(\boldsymbol{\kappa}_f-\mathbf{q}_1)\mathbf{r}} \mid \psi_i^T(\mathbf{r})\rangle \ , \tag{2.5}$$

with $\eta_f = Z_P/\kappa_f$ and $\varepsilon \to +0$. This approximation shall be referred to as the full peaking 2 (FP2) approximation. The difference to the full peaking approximation consists in the appearance of the phase factor

$$\{[q_1^2-(\kappa_f+i\varepsilon)^2]/(\mathbf{q}_1-\boldsymbol{\kappa}_f)^2\}^{-i\eta_f} .$$

Since the phase is real ($q_1>\kappa_f$), this factor does not enter into the total cross section (2.4) for CTC, such that the two peaking approximations become identical. It should be noted that this identity does not hold for the impact-parameter distribution (as will be discussed later on), and also not for the capture into bound states.

Upon insertion of (2.5) into (2.4), the following factorization is obtained:

$$\frac{d^2\sigma^{\mathrm{FP}}}{dE_f\,d\Omega_f}=\frac{2\pi\eta_f}{1-e^{-2\pi\eta_f}}\frac{d^2\sigma^I}{dE_f\,d\Omega_f} ,$$

$$\frac{d^2\sigma^I}{dE_f\,d\Omega_f}=\frac{4Z_P^2k_f}{v}N_i\int d\mathbf{q}_0\,\delta(\tfrac{1}{2}k_f^2-\varepsilon_i^T+\mathbf{q}_0\mathbf{v})\frac{1}{q_0^4}$$

$$\times|\langle\psi^T_{\mathbf{k}_f}(\mathbf{r})|e^{-i\mathbf{q}_0\cdot\mathbf{r}}|\psi_i^T(\mathbf{r})\rangle|^2 . \tag{2.6}$$

In this expression $d^2\sigma^I/dE_f\,d\Omega_f$ is the doubly differential cross section for the ionization of a target electron into a final state with momentum $\mathbf{k}_f$. For reasons of identification, we have introduced the new variable $\mathbf{q}_0=\mathbf{q}_1-\boldsymbol{\kappa}_f$; an explicit evaluation of (2.6) is given in the Appendix. The factorization of the CTC cross section into the ionization cross section times the squared Coulomb normalization factor has first been introduced by Salin[24] from a high-energy CDW-type formulation, and it has also been considered as an approximation to the second-order Born theory for charge exchange.[25] Note that it cannot be strictly derived from the second Born approximation because there the target field is not included to all orders.

This reduction of the impulse approximation has, however, the drawback that the cusp, when calculated from (2.6), turns out to be spherically symmetric in the projectile frame of reference at $\kappa_f=0$, due to the inherent s-wave character of the final state in the full peaking approximation. Unless in the extreme limit $Z_P\ll Z_T$ or $v\gg Z_T$, this approximation therefore does not predict the peak shape correctly.

In order to cope with this deficiency, the transverse peaking approximation is applied to the evaluation of $M(\mathbf{q}_1)$. It consists of replacing $\mathbf{s}_1$ in both the ionization matrix element and the potential by its component parallel to $\mathbf{v}$, while the transverse components are set equal to zero. This approximation relies on the assumption that the momentum transfer proceeds mainly in the longitudinal direction, and it has become quite common for charge transfer into bound states.

However, the evaluation of the transverse-peaked (TP) prior IA is quite complicated for the capture into the continuum if $\mathbf{k}_f$ is not aligned with $\mathbf{v}$. We shall therefore restrict ourselves to the study of just one case, where $\mathbf{k}_f$ is equal to $\mathbf{v}$. This is sufficient to determine the region of applicability of the full peaking approximation, but also to calculate the dominant parameters B_{00} and B_{01}. For $\mathbf{k}_f$ parallel to the z direction $\mathbf{e}_z=\hat{\mathbf{v}}$, the $\mathbf{s}_1$ integrand in (2.3) no longer depends on the azimuthal angle φ_{s_1}, and $M(\mathbf{q}_1)$ becomes

$$M^{\mathrm{TP}}(\mathbf{q}_1)=2\pi\int_0^\infty ds_1\,s_1^2\int_{-1}^{1}dx\frac{1}{q_{1\perp}^2+(s_1x-q_{1z})^2}\varphi^{*P}_{\kappa_f}(\mathbf{s}_1)\langle\psi^T_{s_1x\mathbf{e}_z+\mathbf{v}}(\mathbf{r})|e^{i(s_1x\mathbf{e}_z-\mathbf{q}_1)\mathbf{r}}|\psi_i^T(\mathbf{r})\rangle , \tag{2.7}$$

where we have introduced $x=\cos\vartheta_{s_1}$, and $\mathbf{q}_{1\perp}$ are the components of $\mathbf{q}_1$ perpendicular to $\mathbf{v}$. It is essential to use spherical coordinates in (2.7) in order to obtain the correct result for the integration of $\varphi^{*P}_{\kappa_f}(\mathbf{s}_1)$.

In the limit $\kappa_f\to 0$, $\varphi^{*P}_{\kappa_f}(\mathbf{s}_1)$ simplifies to

$$\varphi^{*P}_{\kappa_f}(\mathbf{s}_1)\to\frac{Z_P}{\pi^2}e^{\pi\eta_f/2}\Gamma(1-i\eta_f)\frac{1}{s_1^4}e^{-2i\lambda Z_Px/s_1} ,$$

$$\lambda=\mathrm{sign}(k_f-v)=(k_f-v)/\kappa_f . \tag{2.8}$$

The step discontinuity of the doubly differential cross section at $\mathbf{k}_f=\mathbf{v}$ is due to the appearance of the phase factor $\exp(-2i\lambda Z_Px/s_1)$, which switches sign when one changes from $k_f=v-0$ to $k_f=v+0$. The dependence on λ survives not only in $M^{\mathrm{TP}}(\mathbf{q}_1)$, but also in the square of it, because $\varphi^P_{\kappa_f}$ is folded with a complex integrand in (2.7). In contrast, in the full peaking 2 approximation, the factor multiplying $\varphi^P_{\kappa_f}$ is real such that $M^{\mathrm{FP2}}(\mathbf{q}_1)$ depends on λ only via a phase which vanishes upon squaring. For details of the numerical evaluation of the doubly differential cross section (2.4) in the transverse peaking approximation, the reader is referred to the Appendix. Also, an explicit expression for $M^{\mathrm{TP}}(\mathbf{q}_1)$ is given there.

B. Impulse approximation in the post form

For heavy projectiles it is the projectile field which has to be included to all orders. Therefore instead of (2.1) one has[17,26]

$$a_{fi}^{\mathrm{post}}=-i\int_{-\infty}^{\infty}dt\int d\mathbf{q}\,\langle\psi_f^P|V_T|\psi_{\mathbf{q}}^P\rangle\langle\mathbf{q}|\psi_i^T\rangle . \tag{2.9}$$

A detailed discussion of the evaluation of (2.9) is given in Ref. 6 and shall not be repeated here. In contrast to the case of bound-bound capture, the evaluation techniques of (2.1) and (2.9) are not the same, because there is an essential difference in the structure of the integrands. Formula (2.1) contains the product of a bound-continuum matrix element and a momentum space continuum state, while in (2.9), which implies the scattering of an electron by the target field, it enters a continuum-continuum matrix element multiplied by a momentum-space bound state. In particular, the continuum-continuum matrix

element [written in Eq. (A7) of the Appendix] is so singular near $\gamma=0$ that the full peaking approximation diverges and thus only the transverse peaking is possible.

III. CALCULATIONS

The calculations have been performed with (nonrelativistic) hydrogenic wave functions (except for the post IA) using a Slater-screened effective charge and experimental binding energies for the target states. For He, $Z_T=1.7$ and $\varepsilon_i^T=-24.98$ eV was used. It had been shown previously[6] that for the ejection into high-energy continuum states, a Hartree-Fock-type approximation for the He states does not introduce significant changes.

In order to compare with experiment, the doubly differential cross section is transformed into the projectile frame. Then an expansion in terms of Legendre polynomials and in powers of κ_f is made,[8,21]

$$\frac{d^2\sigma}{d\varepsilon_f\, d\Omega_f'}=\frac{\kappa_f}{k_f}\frac{d^2\sigma}{dE_f\, d\Omega_f}=\sum_{nl} B_{nl}\kappa_f^n P_l(\cos\theta')\ ,$$
$$\cos\theta'=(\mathbf{k}_f\hat{\mathbf{v}}-v)/\kappa_f\ , \quad (3.1)$$

where $\varepsilon_f=\kappa_f^2/2$, Ω_f' is the electronic solid angle in the projectile frame, and θ' is the angle between $\boldsymbol{\kappa}_f$ and $\mathbf{v}$. At the peak position $\kappa_f=0$, only coefficients B_{0l} enter. If just the monopole and dipole terms are retained, their coefficients can be found in the following way:

$$B_{00}=\frac{1}{2}\left[\frac{d^2\sigma}{d\varepsilon_f\, d\Omega_f'}(k_f=v+0)+\frac{d^2\sigma}{d\varepsilon_f\, d\Omega_f'}(k_f=v-0)\right],$$
$$B_{01}=\frac{1}{2}\left[\frac{d^2\sigma}{d\varepsilon_f\, d\Omega_f'}(k_f=v+0)-\frac{d^2\sigma}{d\varepsilon_f\, d\Omega_f'}(k_f=v-0)\right]. \quad (3.2)$$

It has been shown[12,13] that $l\leq 1$ is sufficient for the light collision systems p, He + He. Also, for protons colliding with heavier targets, such as Ne, there is experimental evidence that higher multipoles are of no significance.

A. CTC from helium targets

In Fig. 1, B_{00} for electron capture from He by protons and α particles, respectively, is shown as a function of projectile energy E_P. Calculations are performed in three different models; the transverse-peaked post IA, as well as the prior IA in full peaking and transverse peaking, respectively. For the prior IA the cross sections are calculated from (A5) and from (2.4) with (A4), respectively, while for the post IA the formulas are given in Ref. 6. It is seen that for the symmetric system, post and prior TP-IA give very close results for the higher velocities; at very large velocities, numerical inaccuracies come into play. For the nonsymmetric p + He system, the post form gives a larger B_{00} than the prior IA, indicating that a strong coupling to the heavier target reduces the cross section. The full peaking approximation overestimates the cross section by at least 20%, even at the highest velocities. The main reason for this lies in the fact that the prior FP-IA reduces asymptotically to the second-Born theory

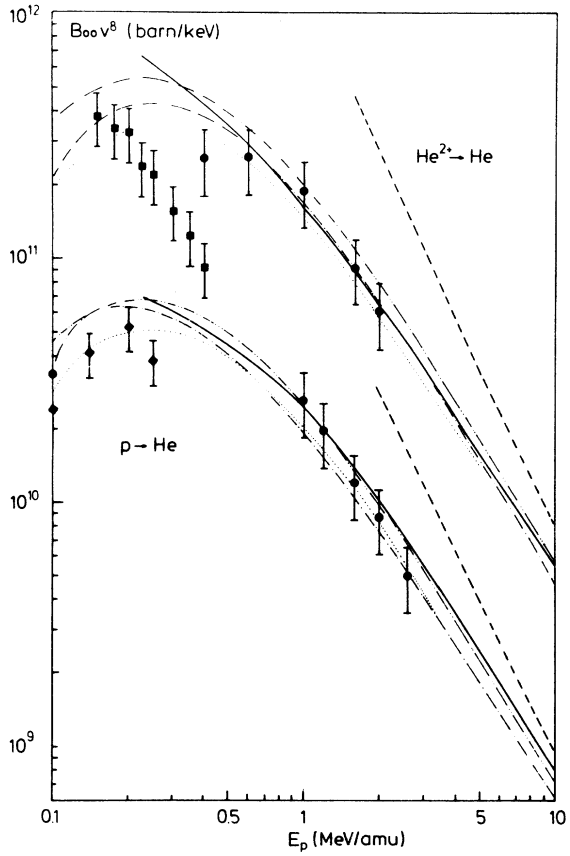

FIG. 1. Intensity parameter B_{00} multiplied by v^8 (v in a.u.) as a function of projectile energy for the systems He^{2+} + He (upper curves) and p + He (lower curves). Shown is the transverse-peaked IA in its post form (——) and its prior form (—·—·—·), as well as the full-peaked prior IA (—··—··—). The dashed line is the high-energy second-Born approximation and the dotted line is a CDW calculation (Ref. 7). Experimental data are from Anderson *et al.* (Ref. 11) (⧫), Dahl (Ref. 9) (⧫), and Berényi (Ref. 14) (⧫).

(or the TP-IA) only up to errors[17] of the order of Z_P/Z_T. For energies above 1 MeV/amu ($v>6.3$ a.u.) the IA agrees well with experimental data from the Aarhus group;[11] at much lower energies, the perturbative treatment inherent in the IA is not expected to be valid any more for these near-symmetry systems.

Comparison is also made with a CDW calculation,[7] which agrees slightly better with the data[9,14] at low velocities. The second Born theory in its high-energy peaking form[3] drastically overestimates the cross section and converges only very slowly to the IA at high v.

A parameter more sensitive to the different theoretical approaches than B_{00} is provided by the asymmetry $\beta=B_{01}/B_{00}$, which is displayed in Figs. 2 and 3. Calculations within the post TP-IA give a much larger β than the prior TP-IA, which demonstrates that a strong coupling to the projectile field amplifies the skewness. That on the other hand a strong coupling to the target field weakens the asymmetry is supported by the fact that the CDW calculation,[7] which includes both potentials exactly (on the expense of the kinetic energy), lies between the

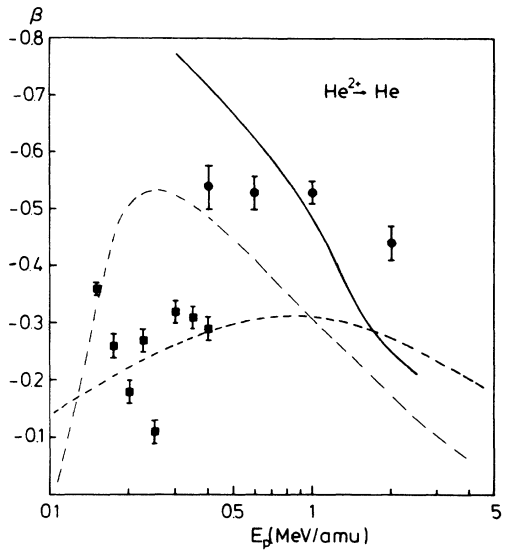

FIG. 2. Asymmetry parameter $\beta = B_{01}/B_{00}$ as a function of projectile energy for $He^{2+} + He$. Shown are calculations within the transverse-peaked post IA (——), the prior IA (—·—·—·), and the peaked second-Born theory (— — —). The experimental data are from Andersen *et al.* (Ref. 11) (ǂ) and Gulyás *et al.* (Ref. 13) (ǂ).

results from the post and prior IA.

At high collision energies the asymmetry tends to zero. This behavior can, in the case of the prior IA, be understood from inspection of (2.7) with (2.8): If the ionization matrix element in (2.7) did not depend on $s_1 x$, the function $\varphi^P_{\kappa_f}(\mathbf{s}_1)$ would be folded with a real expression, such that the λ dependence would drop out of $|M^{\mathrm{TP}}(\mathbf{q}_1)|$. That this actually is true in the limit $v \to \infty$ is based on

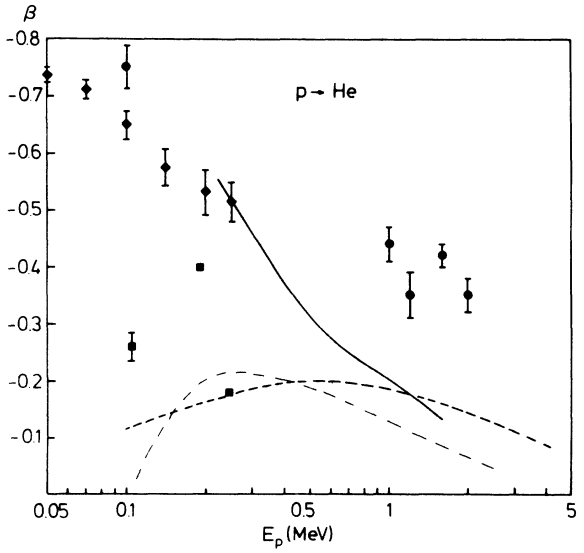

FIG. 3. Asymmetry parameter β as a function of projectile energy for $p + He$. The curves have the same meaning as in Fig. 2, and a CDW calculation (Ref. 7) (· · · ·) is included. Experimental data are from Andersen *et al.* (Ref. 11) (ǂ), Dahl (Ref. 9) (ǂ), and Meckbach *et al.* (Ref. 8) (ǂ).

the fact that the main contribution to $M^{\mathrm{TP}}(\mathbf{q}_1)$ comes from small s_1 and that $q_1 > v/2$, such that the x dependence of the ionization matrix element gradually decreases with increasing v. In the post IA, the asymmetry can be traced back[6] to a discontinuity of the argument in the hypergeometric functions from (A7) entering into the integrand, which varies like Z_P/v. In this context it should be noted that due to convergence problems of these hypergeometric functions the post IA cannot be evaluated sufficiently close to $\kappa_f = 0$; instead, we have chosen a series of finite κ_f on both sides of the peak and extrapolated to $\kappa_f = 0$. This procedure becomes, however, rather inaccurate at high v, causing β to fall even below the peaked second-order Born result (if, for example, both post IA and second Born are calculated at the rather large value $\kappa_f = v/\sqrt{1000}$, the IA approaches the Born theory smoothly from above[11,26]). Also, the prior IA suffers from inaccuracies for high v due to mutual cancellations in $M^{\mathrm{TP}}(\mathbf{q}_1)$ as the x dependence of $F(s_1 x)$ [defined in (A4)] decreases, causing β to drop too strongly with v. The parameter β is much more subject to the numerical deficiencies than the absolute cross section (Fig. 1). Other theoretical results concern the increase of β with Z_P [because the strength of the discontinuity is proportional to Z_P; see also (2.8)], but the lack of any scaling property of β with E_P/Z_P which had been suggested from experimental evidence.[11,12]

The selection of one theory by means of comparison with experiment is complicated by the fact that the data from the different groups[8,9,11,13] do not show a unique dependence on the collision energy. The Aarhus data[9,11] seem to give preference to the post IA. At low impact energies, however, the asymmetry predicted by this theory is too large[12] for projectiles with $Z_P \geq 2$. On the other hand, a weak coupling to the projectile field (prior IA) substantially underestimates β, especially for the $p + He$ system. The complete breakdown of the prior IA is reached around $E_P = 0.1$ MeV/amu, where β even changes sign. Evidently, it is a strong coupling to both potentials (but not within the CDW scheme) which becomes important in slow collisions.

B. CTC from neon targets

For proton impact on heavier targets, we have only applied the prior IA. It is straightforward to generalize this theory to include capture from higher shells because one can use the matrix elements well-known from ionization theories. In the special case of the L subshells, these matrix elements are listed in the Appendix.

In Fig. 4, B_{00} values for the Ne subshells are given as a function of the collision velocity. The falloff with v due to the increasing minimum momentum transfer $q_{\min}$ is much stronger for the L shell that it is for the K shell. For collision velocities above the initial electronic orbiting velocity, the full peaking approximation differs from the transverse peaking approximation in general by less than 20%, the only exception being for the $2p, m = 1$ state. For this state, transverse momentum transfer is important and thus its partial neglect in the FP-IA is justified to a much lesser extent.

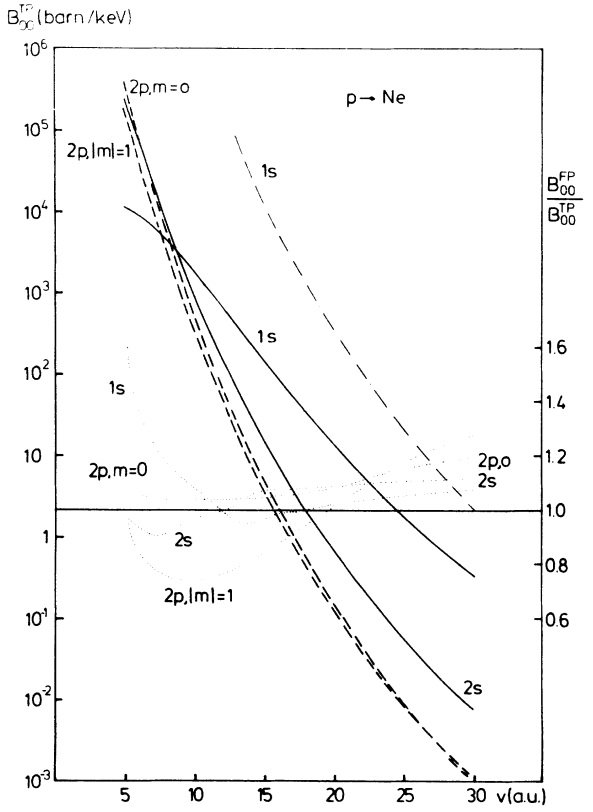

FIG. 4. B_{00} in the transverse-peaked prior IA (left-hand scale) for $p+\mathrm{Ne}$ as a function of collision velocity v. The solid lines are the contribution from the Ne $1s$ and $2s$ states, the dashed lines are the $2p,m=0$ and the $2p,|m|=1$ contributions. Also shown is B_{00} for the $1s$ state in the peaked second-Born approximation (dot-dashed line). The dotted curves give the ratio of B_{00} calculated in the full-peaked and the transverse-peaked IA, respectively (right-hand scale).

The skewness parameter β is plotted in Fig. 5. Interestingly, for the higher collision velocities only the s states exhibit a negative β, while for the p states β is positive, indicating that electrons with velocity slightly above the peak are ejected with more intensity than those with $k_f < v$. This feature is related to the structure of the p-

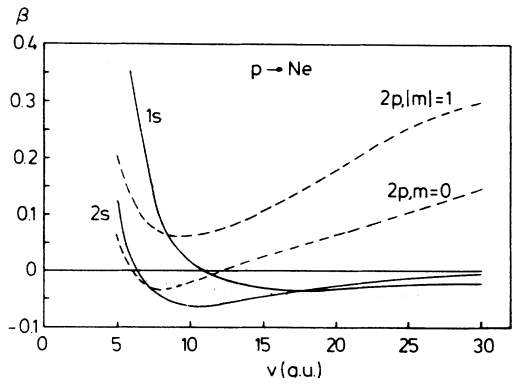

FIG. 5. β for the $p+\mathrm{Ne}$ system as a function of collision velocity in the transverse-peaked prior IA (solid lines, target $1s$ and $2s$ states; dashed lines, target $2p$ states) and in the peaked second-Born theory (dotted line, target $1s$ state).

state wave function. The strong increase of β in the positive regime for velocities below 10 a.u. again indicates the breakdown of a first-order theory in V_P. Comparison is also made with the high-velocity second Born approximation[3] for the $1s$ state, which gives a quite reasonable β, although the absolute cross section, i.e., B_{00}, is far too high.

For the calculation of the electron spectrum with arbitrary κ_f, the transverse peaking approximation requires much numerical effort. We therefore suggest correcting the full peaking approximation for its deficiency of yielding $\beta=0$ by means of including a β which has been determined from the TP-IA, and also by adjusting B_{00} to the value from the TP-IA. This leads to the following formula:

$$\frac{d^2\sigma}{dE_f\,d\Omega_f} \approx \frac{k_f}{\kappa_f} B_{00}^{\mathrm{TP}} \left[(1+\beta\cos\theta') + \frac{1}{B_{00}^{\mathrm{FP}}} \sum_{n\geq 1} \sum_{l} B_{nl}^{\mathrm{FP}} \kappa_f^n P_l(\cos\theta') \right] = \frac{k_f}{\kappa_f} \left[\frac{B_{00}^{\mathrm{TP}}}{B_{00}^{\mathrm{FP}}} \frac{d^2\sigma^{\mathrm{FP}}}{d\varepsilon_f\,d\Omega_f'} + B_{00}^{\mathrm{TP}} \beta\cos\theta' \right] . \quad (3.3)$$

Into (3.3) enters the assumption that the relative dependence on κ_f is to sufficient accuracy determined by the full peaking approximation. This assumption may be justified from the fact that even for finite κ_f, the function $\varphi_{\kappa_f}^{P}(\mathbf{s}_1+\boldsymbol{\kappa}_f)$ diverges strongly in $s_1=0$ (like s_1^{-3}). Thus the quality of the full peaking approximation depends only weakly on κ_f as long as κ_f is small compared to v.

Figure 6 shows the forward peak for all Ne subshells in

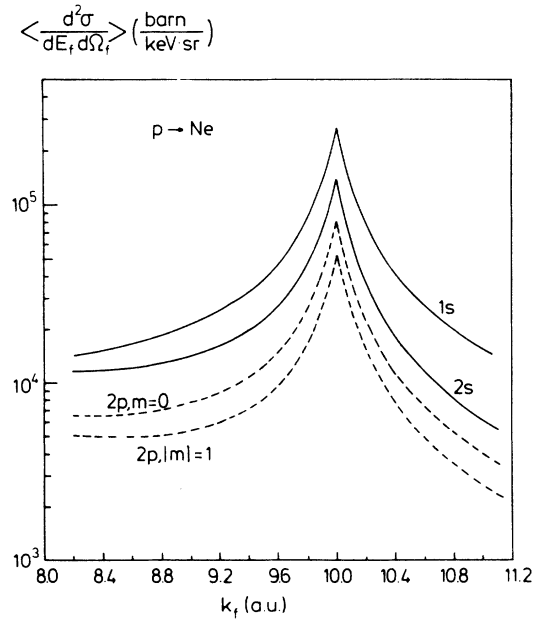

FIG. 6. Doubly differential cross section for cusp electron emission, averaged over the detector resolution $\theta_0=0.75°$ for 2.5-MeV $p+\mathrm{Ne}$ ($v=10.005$ a.u.) collisions as a function of electron momentum k_f. Shown are the contributions from the target $1s$ and $2s$ states (——) and from the $2p$ states (— — —) calculated in the asymmetry-corrected full-peaked prior IA, Eq. (3.3).

this approximation for an impact velocity of 10 a.u., averaged over the angular resolution θ_0. At this velocity the subshell spectra are nearly symmetric at half maximum ($|\beta| \lesssim 0.06$), but it becomes clear that in the wings, where higher powers of κ_f come into play, the L subshells show a strong enhancement on the low-energy side. This follows from the behavior of the ionization cross section (2.6), which constitutes the slowly varying "background" in the cusp region. Furthermore, the contribution of the summed L shell is about as large as the contribution from the K shell.

It should be noted that there is no cusp inversion for the $2p,m=0$ state for CTC, in contrast to the case for electron loss to the continuum.[27] The reason lies in the fact that for charge transfer the average momentum transfer is always of the order of v, i.e., large, such that small variations of κ_f around 0 hardly alter the relevant electron momenta entering from the $2p,m=0$ initial state. Thus it is always the Coulomb normalization factor which dominates the cusp shape.

Experiments with a very high resolution are presently under investigation for various projectile-target combinations.[20] In Fig. 7 the experimental cusp spectrum for 4.2-MeV p colliding with Ne is compared with calculations where $d^2\sigma/dE_f\,d\Omega_f$ is averaged over the experimental resolution ($\theta_0=0.75°$, $\Delta E_f/E_f=0.5\%$). The deviation between experiment and the summed $K+L$ shell calculation is about 25% and lies within the experimental accuracy of the absolute values. However, the experiment shows a much larger asymmetry than theory even if the TP-corrected formula (3.3) is used. This effect is still more pronounced if the proton velocity is lowered. The reason is not yet clear. Tentatively, the enhanced number of electrons emerging with $k_f<v$ may be explained by means of a double-scattering mechanism which would lead to a redistribution of the CTC electrons. A thorough experimental study of the peak shape is in progress.

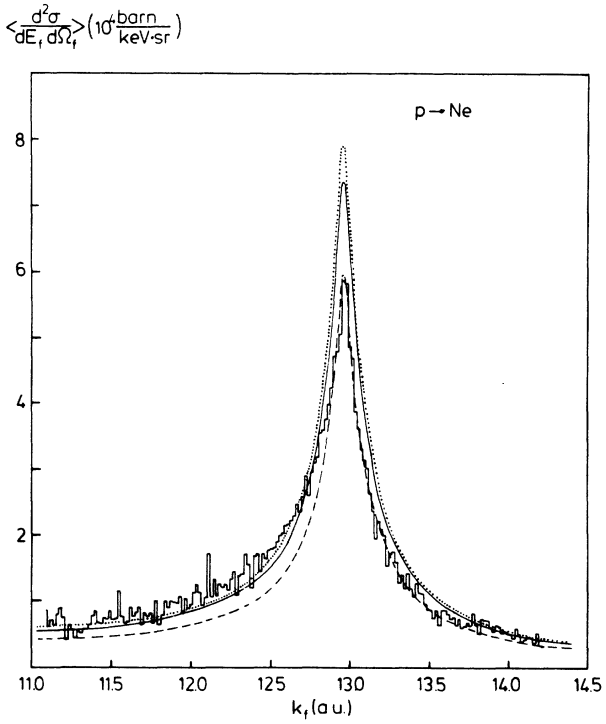

FIG. 7. Doubly differential cross section for cusp electron emission, averaged over the experimental angular resolution ($\theta_0=0.75°$) and energy resolution ($\Delta E_f/E_f=0.005$) for 4.2-MeV $p+$Ne ($v=12.97$ a.u.) collisions as a function of electron momentum k_f. The experimental data from Schramm *et al.* (Ref. 20) (histogram) are compared with the full-peaked (——) and the asymmetry-corrected full-peaked (· · · ·) prior IA, summed over all target shells. Also given is the 1s contribution in the full-peaked prior IA (— — —).

$$\frac{d^2P}{dE_f\,d\Omega_f}=k_f\frac{N_i}{2\pi}\int_0^{2\pi}d\varphi_f\,|a_{fi}(b)|^2\,, \tag{3.4}$$

where N_i is the number of electrons in the subshell i and where the average is taken over the experimentally unobserved azimuthal angle φ_f. In particular, the FP2 approximation gives

C. Impact-parameter dependence and alignment

So far, no studies of the impact-parameter dependence of cusp electrons have been performed. The b dependence is obtained from the formula

$$a_{fi}^{\mathrm{FP2}}(b)=\frac{iZ_P}{\pi v}e^{\pi\eta_f/2}\Gamma(1-i\eta_f)\int_{q_{\min}}^{\infty}q_1\,dq_1\int_0^{2\pi}d\varphi_{q_1}\,e^{iq_1 b\sin\vartheta_{q_1}\cos\varphi_{q_1}}\frac{1}{(\mathbf{q}_1-\boldsymbol{\kappa}_f)^2}\left[\frac{q_1^2-\kappa_f^2}{(\mathbf{q}_1-\boldsymbol{\kappa}_f)^2}\right]^{-i\eta_f}$$

$$\times\langle\psi_{\mathbf{k}_f}^T(\mathbf{r})\,|\,e^{i(\boldsymbol{\kappa}_f-\mathbf{q}_1)\mathbf{r}}\,|\,\psi_i^T(\mathbf{r})\rangle\,, \tag{3.5}$$

while in the FP approximation the phase factor in the first line of (3.5) is missing. In the limit $\kappa_f\to 0$, the integral over φ_{q_1} leads to a Bessel function $J_{|m|}$, where m is the magnetic quantum number of the initial state, and also the dependence on φ_f drops out. With the transverse peaking approximation, one obtains in this case

$$\frac{d^2P^{\mathrm{TP}}}{dE_f\,d\Omega_f}=\frac{32Z_P^5}{\kappa_f v\pi}N_i\left|\int_{q_{\min}}^{\infty}dq_1\,q_1 J_{|m|}(q_1 b\sin\vartheta_{q_1})\int_0^{\infty}\frac{ds_1}{s_1^2}\int_{-1}^{1}dx\,e^{-2i\lambda Z_P x/s_1}\frac{1}{q_{1\perp}^2+(s_1x-q_{1z})^2}\right.$$
$$\left.\times\langle\psi^T_{s_1xe_z+v}(\mathbf{r})\,|\,e^{i(s_1xe_z-q_1)\cdot r}\,|\,\psi_i^T(\mathbf{r})\rangle e^{-im\varphi_{q_1}}\right|^2. \tag{3.6}$$

In (3.6), use has been made of the fact that the ionization matrix element depends on φ_{q_1} only via the phase $\exp(im\varphi_{q_1})$, which has been included in the integration over φ_{q_1}.

The impact-parameter dependence of the transition probability at $k_f=v+0$ for 2.5-MeV p colliding with Ne is shown in Fig. 8. Comparison is made between the TP, FP, and FP2 impulse approximation. For the s states, the FP2-IA as well as the FP-IA are satisfactory, except for very large b and in the dip resulting from the nodal structure of the $2s$ state. The $2p$ states show an oscillatory behavior with b and for these states the full peaking and FP2 approximations are not so good. In particular, these approximations lead to a spurious structure in the $2p, m=1$ transition probability around $b\approx 0.1$ a.u., which is smoothed in the TP approximation (3.6) due to the inclusion of more than one intermediate electronic continuum states.

The oscillation of the p-state transition probability becomes more evident if the alignment is considered,

$$A_{20}=\frac{\frac{1}{2}P_{|m|=1}-P_{m=0}}{P_{|m|=1}+P_{m=0}}, \tag{3.7}$$

where P stands for $d^2P/dE_f\,d\Omega_f(b)$. Figure 9 shows that there are oscillations in $A_{20}(b)$ as a function of b. From their period Δb the frequency can be derived via $k=2\pi/\Delta b$, and it is about equal to the collision velocity v (which in the case considered agrees with the electron velocity k_f). These oscillations can be traced back to the out-of-phase oscillations of the Bessel functions J_0 and J_1 entering into (3.6). Since from the ionization matrix element it follows that $q_1\approx v$ at high v, this thus constitutes the natural oscillation frequency. It is evident from (2.6) that the alignment for ionization into a given final state $\mathbf{k}_f$ is identical to the one calculated in the FP approximation for capture. From Fig. 9 it follows that the oscillations are present not only for capture, but also for ionization, although with somewhat shifted phase. If k_f is chosen to be much greater than v, the oscillations are

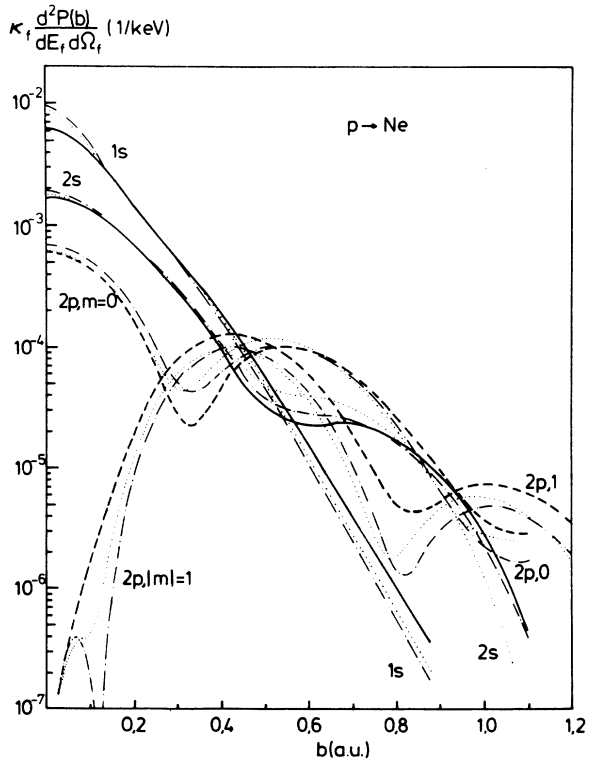

FIG. 8. Impact-parameter dependence of the CTC probability times κ_f (κ_f in a.u.) for $p+$Ne collisions. The electron momentum $\mathbf{k}_f$ equals $\mathbf{v}$ ($v=10$ a.u.). Solid and dashed lines, transverse-peaked prior IA for target s and p states, respectively. Also shown is the IA in full peaking (· · · ·) and in the full peaking 2 approximation (—·—·—·).

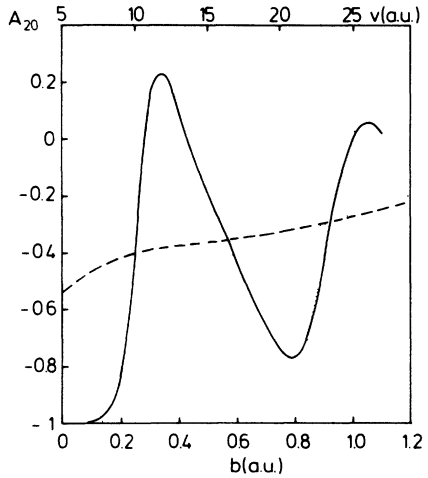

FIG. 9. Alignment A_{20} for the Ne L shell in $p+$Ne collisions as a function of impact parameter at fixed velocity $v=10$ a.u. (lower scale); solid line, transverse-peaked prior IA; dotted line, full-peaked prior IA. Also shown is the total alignment as a function of velocity (upper scale); dashed line, transverse-peaked prior IA; dotted line, full-peaked prior IA. In all calculations, $\kappa_f=0$.

damped, while for k_f much smaller than v, the oscillation frequency is lowered correspondingly, but there is again a strong damping at the higher b.

Also shown in Fig. 9 is the impact-parameter integrated alignment [where P in (3.7) is replaced by $d^2\sigma/dE_f\,d\Omega_f$] as a function of the collision velocity. The p states are less aligned when v is increased. This increase in A_{20} is related to the fact that for small v ($v \approx Z_T$), the main contribution to the q_1 integral in (2.4) comes from $q_1 \approx q_{\min} \approx v$. Thus capture from the $|m|=1$ states is suppressed, because these states relate to the transverse momentum transfer $\sin^2\vartheta_{q_1} = q_1^2 - q_{\min}^2$ (see Appendix), which results in A_{20} being strongly negative. For high velocities, $q_1 \approx v$, but $q_{\min} \simeq v/2$, such that the $|m|=1$ states are favored, which produces a smaller alignment. It should be pointed out that A_{20} is exclusively determined from the differential cross section at the cusp ($\mathbf{k}_f = \mathbf{v}$): The alignment does not change if one averages over the angular resolution, or even if one energy integrates over the forward peak.

D. Capture into Rydberg states and comparison with CTC

The prior impulse approximation in the full peaking and FP2 approximation is readily extended to capture into high-lying Rydberg states. The only change in the transition amplitude (2.3) is the replacement of the momentum-space Coulomb wave φ_f^P by the Fourier-transformed Rydberg-state wave function φ_{nlm}^P, of the energy $\kappa_f/2$ by $\varepsilon_n^P = -Z_P^2/2n^2$, and of κ_f by 0 in $M(\mathbf{q}_1)$. In the FP2 approximation, the cross section for capture into the projectile state with quantum numbers nlm is given by

$$\sigma_{nlm}^{\mathrm{FP2}} = \frac{4Z_P^2}{v} N_i \int d\mathbf{q}_1\, \delta(\varepsilon_n^P - \varepsilon_i^T + \mathbf{q}_1\mathbf{v} + v^2/2) \times |M_{nlm}^{\mathrm{FP2}}(\mathbf{q}_1)|^2 ,$$

$$M_{nlm}^{\mathrm{FP2}}(\mathbf{q}_1) = \langle \psi_{\mathbf{v}}^T(\mathbf{r}) | e^{-i\mathbf{q}_1\cdot\mathbf{r}} | \psi_i^T(\mathbf{r}) \rangle \times \int d\mathbf{s}_1 \frac{1}{(\mathbf{s}_1 - \mathbf{q}_1)^2} \varphi_{nlm}^{*P}(\mathbf{s}_1) . \quad (3.8)$$

If one is interested in the total capture into a given shell n, (3.8) has to be summed over l and m. This summation can be directly performed on the squared $M_{nlm}^{\mathrm{FP2}}(\mathbf{q}_1)$, and one obtains

$$\sum_{l,m} |M_{nlm}^{\mathrm{FP2}}(\mathbf{q}_1)|^2 = 2\pi^2 |\langle \psi_{\mathbf{v}}^T(\mathbf{r}) | e^{-i\mathbf{q}_1\cdot\mathbf{r}} | \psi_i^T(\mathbf{r}) \rangle|^2 \times \sum_{l=0}^{n-1} (2l+1) |G_{nl}(q_1)|^2 ,$$

$$G_{nl}(q_1) = \int_0^\infty dr\, r R_{nl}^*(r) j_l(q_1 r) . \quad (3.9)$$

In this expression, R_{nl} is the radial part of the Rydberg-state wave function and j_l is a spherical Bessel function. Due to the summation over m, only the radial integral $G_{nl}(q_1)$ enters, and there is no dependence on the direction of $\mathbf{q}_1$ left. For hydrogenic wave functions, $G_{nl}(q_1)$ is given in the Appendix. It is nonzero for any l, but for $Z_P \ll Z_T$, the s states largely dominate. In the full peaking approximation, on the other hand, where $(\mathbf{s}_1 - \mathbf{q}_1)^{-2}$ in (3.8) is replaced by q_1^{-2}, $M_{nlm}^{\mathrm{FP}}(\mathbf{q}_1)$ becomes proportional to the Rydberg function at the origin, which vanishes for $l > 0$. Thus for capture into bound states, the FP2 approximation should be preferred.

For large n, the cross section $\sigma_n = \sum_{l,m} \sigma_{nlm}$ scales very accurately with n^{-3}. From the continuity at the projectile ionization threshold, a relation between σ_n and B_{00} can be derived,[21] which reads, when generalized to arbitrary projectile charges,[22,23]

$$B_{00} = \frac{1}{4\pi Z_P^2} \sigma_n n^3 \quad \text{as } n \to \infty . \quad (3.10)$$

This parameter can be used to test the accuracy of the calculations. In the full peaking approximation for capture from the K shell, we have found very good agreement ($\ll 1\%$) between the B_{00} from (3.10) and the one from integration of (3.1) for a series of projectile-target combinations. However, when the FP2 approximation is used, the deviations are about 2% for the p + Ne system, but considerably larger for greater projectile charges, especially at low collision velocities. The difference is exclusively due to the population of $l \neq 0$ bound states in the FP2 theory. This is an example that the continuity across threshold is not automatically fulfilled if approximations are introduced into the theory.

A question of interest is the population of Rydberg states as compared to low-lying continuum states, when the projectiles has left the target. Due to the n^{-3} scaling, the cross section for capture into Rydberg states with $n \geq n_0$, where n_0 is some fixed shell number, can be written in the following way:

$$\sigma_{n_0}^{\mathrm{Ryd}} = \sum_{n \geq n_0}^{\infty} \sigma_n = \left[\zeta(3) - \sum_{n=1}^{n_0-1} n^{-3} \right] \{\sigma_n n^3\}_{n\to\infty} , \quad (3.11)$$

where ζ is the zeta function with $\zeta(3) = 1.202\ldots$, and $n_0 \gtrsim 5$. For p + Ne, (3.11) holds even for $n_0 = 1$ within 5%. This is compared with the CTC cross section, integrated over energy and angle,

$$\sigma_{\mathrm{CTC}} = 2\pi \int_{E_{\min}}^{E_{\max}} dE_f \int_0^{\theta_0} d\theta \sin\theta \frac{d^2\sigma}{dE_f\, d\Omega_f} . \quad (3.12)$$

We have compared $\sigma_{n_0}^{\mathrm{Ryd}}$ and σ_{CTC} for K-shell capture from Ne by protons. For the limits of integration we have taken an electron energy which corresponds to the momentum $v \pm 0.05v$, and which covers most of the peak region. The cross section (3.12) shows, however, a strong dependence on the angular resolution θ_0. While the angular averaged cross section exhibits only a slight decrease with θ_0, there appears an additional factor of $1 - \cos\theta_0 \approx \theta_0^2/2$ from the θ integration. For p + Ne, one has approximately $\sigma_{\mathrm{CTC}} \sim \theta_0^{1.6}$ for $\theta_0 \lesssim 2°$, independent of the collision velocity v.

Table I shows the ratio $R = \sigma_{\mathrm{CTC}}/\sigma_{n_0}^{\mathrm{Ryd}}$ as a function of n_0. While at any velocity, most of the electrons are captured into the ground state, the capture to the continuum

TABLE I. Total capture cross sections from the Ne K shell into Rydberg states of hydrogen with $n \geq n_0$, $\sigma_{n_0}^{\mathrm{Ryd}}$, and into the continuum, σ_{CTC} (with $\theta_0 = 1°$) in the FP2 approximation. Also shown is the ratio $R(v) = \sigma_{\mathrm{CTC}}/\sigma_{n_0}^{\mathrm{Ryd}}$ as a function of the collision velocity v. Numbers in square brackets denote powers of ten.

v (a.u.)	n_0	$\sigma_{n_0}^{\mathrm{Ryd}}$ (barn)	σ_{CTC} (barn)	$R(v)$	$R(v)/R(v=7)$
7	1	3.59[3]		1.42[−2]	
	11	1.39[1]	5.09[1]	3.67	1
	51	6.01[−1]		8.47[1]	
10	11	3.03	2.27[1]	7.50	2.04
15	11	2.32[−1]	3.93	1.70[1]	4.62
20	11	2.29[−2]	6.94[−1]	3.03[1]	8.25

exceeds $\sigma_{n_0}^{\mathrm{Ryd}}$ for n_0 higher than 10 already by one order of magnitude. Also given in Table I is the relative velocity dependence of R, which is a universal quantity, as it is independent of n_0 and θ_0. The population of continuum states relative to the Rydberg states increases strongly with velocity, because the available energy space in the continuum gets larger. The proportionality of the integration interval $E_{\max} - E_{\min}$ to v^2 thereby leads to an approximate increase of R with v^2.

IV. CONCLUSION

We have studied the intensity and the shape of the forward peak within the prior and post forms of the peaked impulse approximation. We have found that for the symmetric system $He^{2+} + He$, the prior and post IA's give identical results at high velocity within the numerical accuracy, although their evaluation schemes are completely different. In both versions, the peak is skewed towards the low-energy side, but considerably more in the post version which includes the coupling to the projectile field to all orders. Thus the post-prior agreement for the skewness parameter β is only reached at a much larger velocity than for the intensity parameter B_{00}. At not too low velocities, experimental data seem to favor the post IA, but the large spread in the data does not allow for a definite conclusion. Even for the weak asymmetric $p + He$ system, the post IA agrees somewhat better with the data. From this it must be concluded that a single coupling to the projectile field, as inherent in the prior IA, underestimates the peak asymmetry even when $Z_P < Z_T$.

For the strongly asymmetric $p + Ne$ system, however, the prior IA gives a very good agreement with experimental data at the higher collision velocities. For this system, capture from the target L shell becomes increasingly important when v is lowered. While the $2s$ state produces a peak which is likewise skewed towards the low-energy side, the cusp originating from the $2p$ states is in a large velocity region skewed towards the high-energy side at half maximum. However, for this asymmetric system the skewness is very small and the p-state behavior is thus difficult to observe experimentally, especially because the s states (except at very low velocity) give the dominant contribution to the total intensity. The small skewness allows, however, for a simplified description of the capture to continuum in terms of a scaled doubly differential target ionization cross section, where the electron is ejected with momentum $\mathbf{k}_f$. This model, which emerges from the full peaked prior IA, provides only a symmetric peak, but apart from that it shows all essential features of CTC. In particular, it reproduces the oscillations of the impact-parameter-dependent transition probability for the $2p$ initial states, which become even more pronounced in the b-dependent alignment. These oscillations show a resonantlike behavior for electron momenta $k_f \simeq v$, but are damped when k_f is much different from v.

The doubly differential CTC cross section in the projectile frame at the continuum threshold can be related to the cross section for capture into high-n projectile Rydberg states. When a comparison is made between the angle- and energy-integrated CTC cross section and the cross section for capture into arbitrary Rydberg states with $n \geq n_0$, it is found that for a collision system with very light projectiles, such as $p + Ne$, only a very small portion of electrons is captured into high-lying Rydberg states with, say, $n_0 > 20$. The portion becomes still smaller when v is increased. This result is in accord with the experimental observation that for very energetic $Ne^{10+} + Ne$ collisions, the fraction of ECC electrons detected behind the target exceeds by far the fraction of electrons captured into a broad band of high-lying Rydberg states.[28]

ACKNOWLEDGMENTS

I would like to thank H.-D. Betz for stimulating this project, and W. Oswald for many discussions about experimental details and for the data reduction prior to publication. Financial support from Gesellschaft für Schwerionenforschung Darmstadt m.b.H. is gratefully acknowledged.

APPENDIX

In this appendix we give explicit expressions for the matrix elements and cross sections for capture from the target K and L shell into the continuum and into Rydberg states of the projectile, which relate to the prior impulse approximation. Also, the continuum-continuum

scattering matrix element occurring in the post IA is given.

Let us denote by I_i the following integral:

$$I_i(\mathbf{k},\mathbf{p},\mathbf{q})=\langle \psi_{\mathbf{k}}^T(\mathbf{r}) \mid e^{i(\mathbf{p}-\mathbf{q})\cdot\mathbf{r}} \mid \psi_i^T(\mathbf{r})\rangle \ . \tag{A1}$$

With the appropriate choice of the variables $\mathbf{k}$, $\mathbf{p}$, and $\mathbf{q}$, I_i appears in the integrands both for CTC and for capture into bound states, if the prior impulse approximation is used.

Let us define

$$\begin{aligned}
A_n&=(\mathbf{p}-\mathbf{q})^2-(k+iZ_T/n)^2 \ ,\\
B_n&=Z_T^2/n^2+(\mathbf{q}-\mathbf{p}+\mathbf{k})^2 \ ,\\
M_1&=(1-i\eta_k)[(2+i\eta_k)+(2-i\eta_k)A_2/B_2] \ ,\\
M_2&=(1-i\eta_k)i\eta_k+(2+i\eta_k)(1+i\eta_k)B_2/A_2 \ ,\\
N_0&=(2^{3/2}/\pi)Z_T^{5/2}e^{\pi\eta_k/2}\Gamma(1-i\eta_k) \ ,
\end{aligned} \tag{A2}$$

with $\eta_k=Z_T/k$. Then the integrals for the various initial states are given by

$$\begin{aligned}
I_{1s}(\mathbf{k},\mathbf{p},\mathbf{q})&=N_0(A_1^{-i\eta_k}/B_1^{2-i\eta_k})[(1+i\eta_k)B_1/A_1+(1-i\eta_k)] \ ,\\
I_{2s}(\mathbf{k},\mathbf{p},\mathbf{q})&=2^{-5/2}N_0(A_2^{-i\eta_k}/B_2^{2-i\eta_k})\{(1+i\eta_k)[2B_2/A_2+(i/2)Z_Tk(2+i\eta_k)^2B_2/A_2^2]\\
&\quad+(1-i\eta_k)[2-Z_T^2(2+i\eta_k)/A_2-(Z_T^2/2)(2-i\eta_k)/B_2]\} \ ,\\
I_{2p,\,m=0}(\mathbf{k},\mathbf{p},\mathbf{q})&=-i2^{-5/2}N_0Z_T(A_2^{-i\eta_k-1}/B_2^{2-i\eta_k})[M_1k\cos\vartheta_k+(M_1+M_2)(q\cos\vartheta_q-p\cos\vartheta_p)]\\
I_{2p,\,m=1}(\mathbf{k},\mathbf{p},\mathbf{q})&=i2^{-3}N_0Z_T(A_2^{-i\eta_k-1}/B_2^{2-i\eta_k})[M_1k\sin\vartheta_ke^{i\varphi_k}+(M_1+M_2)(q\sin\vartheta_qe^{i\varphi_q}-p\sin\vartheta_pe^{i\varphi_p})] \ ,
\end{aligned} \tag{A3}$$

where the z direction is taken along $\mathbf{v}$. Q, ϑ_Q, and φ_Q are the spherical coordinates of any vector $\mathbf{Q}$.

In the evaluation of the transverse peaked IA, Eq. (2.7) with (2.8), the pole structure of the integrand has to be considered carefully. There is a weak singularity at $(s_1x-q_{1z})^2+q_{1\perp}^2=0$, which can easily be dealt with if the lower limit of the q_1 integration is chosen slightly above $q_{\min}$. Furthermore, there is a square-root singularity in the x integral at $s_1x+v=0$, for $s_1>v$, which is due to the normalization factor of the target Coulomb wave. It can be handled by means of a logarithmic variable substitution in the regions $-1<x<-v/s_1$ and $-v/s_1<x<0$. A very strong, but integrable singularity appears in the s_1 integral at $s_1=0$. This singularity has to be extracted by hand and its integral performed analytically. Coping with the additional difficulty of a rather slow falloff for $s_1\to\infty$, the integral is split at some intermediate $\bar{s}_1$ (which was taken to be $\bar{s}_1=v/2$) and the substitution $s_2=1/s_1$ is made for $s_1>\bar{s}_1$. Then $M^{\mathrm{TP}}(\mathbf{q}_1)$ can be written in the following way:

$$\begin{aligned}
M^{\mathrm{TP}}(\mathbf{q}_1)&=\int_0^\infty\frac{ds_1}{s_1^2}\int_{-1}^1dx\,e^{-2i\lambda Z_Px/s_1}F(s_1x)\\
&=F(0)\pi/(2Z_P)+\int_0^{\bar{s}_1}\frac{ds_1}{s_1^2}\int_{-1}^1dx\,e^{-2i\lambda Z_Px/s_1}[F(s_1x)-F(0)]\\
&\quad+\int_0^{1/\bar{s}_1}ds_2\int_{-1}^1dx\,e^{-2i\lambda Z_Pxs_2}[F(x/s_2)-F(0)] \ ,
\end{aligned} \tag{A4}$$

with

$$\begin{aligned}
F(s_1x)&=(2Z_P/\pi)e^{\pi\eta_f/2}\Gamma(1-i\eta_f)\frac{1}{q_{1\perp}^2+(s_1x-q_{1z})^2}\\
&\quad\times I_i(s_1x\mathbf{e}_z+\mathbf{v},s_1x\mathbf{e}_z,\mathbf{q}_1) \ .
\end{aligned}$$

In addition, a logarithmic variable substitution $y=\ln s_1$ should be used, and the lower integration limits 0 should be replaced by some small, but finite ε.

In the full peaking approximation, there are no numerical difficulties. From (2.6), it follows that

$$\begin{aligned}
\frac{d^2\sigma^{\mathrm{FP}}}{dE_f\,d\Omega_f}&=\frac{8\pi Z_P^2k_f\eta_f}{v^2(1-e^{-2\pi\eta_f})}N_i\\
&\quad\times\int_{q_{0\min}}^\infty dq_0\frac{1}{q_0^3}\int_0^{2\pi}d\varphi_{q_0}\mid I_i(\mathbf{k}_f,0,\mathbf{q}_0)\mid^2 \ ,
\end{aligned} \tag{A5}$$

with $q_{0\min}=(k_f^2/2-\varepsilon_i^T)/v$ and $\cos\vartheta_{q_0}=-q_{0\min}/q_0$.

For the capture into a bound projectile state n,l (summed over m), one has from (3.8)

$$\sigma_{nl}=\frac{16\pi^3 Z_P^2}{v^2}N_l\int_{Q_{\min}}^{\infty}dq_1\, q_1(2l+1)\,|\,G_{nl}(q_1)\,|^2\,|\,I_l(\mathbf{v},0,\mathbf{q}_1)\,|^2\ ,$$

$$G_{nl}(q)=N_l q^l(Z_P/n-iq)^{n-2l-2}(Z_P/n+iq)^{-n}{}_2F_1(l+1,-n+l+1,2l+2,-[(4iqZ_P/n)/(Z_P/n-iq)^2])\ ,$$

$$N_l=(-1)^{n-l-1}\frac{Z_P^{l+3/2}}{n^{l+2}\Gamma(l+\frac{3}{2})}\left[\frac{\pi(n+l)!}{(n-l-1)!}\right]^{1/2}\ , \tag{A6}$$

with $Q_{\min}=(\varepsilon_n^P-\varepsilon_i^T+v^2/2)/v$ and $\cos\vartheta_{q_1}=-Q_{\min}/q_1$. The total capture cross section σ_n into the shell n is obtained from (A6) by summing over l $(0\le l\le n-1)$.

For the evaluation of the post IA, the scattering matrix element of continuum projectile states is needed,[6]

$$\begin{aligned}\langle\psi_{\kappa_f}^P\,|\,e^{i\mathbf{s}\cdot\mathbf{r}}\,|\,\psi_{\mathbf{q}}^P\rangle=&-\frac{1}{(2\pi)^2}e^{\pi\eta_f/2}\Gamma(1-i\eta_f)e^{-\pi\eta_q/2}\Gamma(1-i\eta_q)\alpha^{i\eta_q-1}\gamma^{i\eta_f-i\eta_q-1}(\gamma+\delta)^{-i\eta_f-1}\\&\times\Big[{}_2F_1(1-i\eta_q,i\eta_f,1;[(\alpha\delta-\beta\gamma)/\alpha(\gamma+\delta)])[\eta_f(\kappa_f\gamma-q\delta)+Z_P(\gamma+\delta)]\\&+{}_2F_1(2-i\eta_q,1+i\eta_f,2;[(\alpha\delta-\beta\gamma)/\alpha(\gamma+\delta)])\frac{(1-i\eta_q)\gamma\eta_f}{\alpha(\gamma+\delta)}\\&\times[q\delta(\alpha+\beta)-\kappa_f\gamma(\alpha+\beta+\gamma+\delta)]\Big]\ ,\end{aligned} \tag{A7}$$

where $\eta_q=Z_P/q$, ${}_2F_1(a,b,c;z)$ is a hypergeometric function, and the following abbreviations are used:

$$\begin{aligned}&\alpha=(\mathbf{q}+\mathbf{s}-\boldsymbol{\kappa}_f)^2/2,\quad \beta=\boldsymbol{\kappa}_f(\mathbf{q}+\mathbf{s}-\boldsymbol{\kappa}_f)-i\varepsilon\ ,\\&\gamma=q^2/2-(\mathbf{s}-\boldsymbol{\kappa}_f)^2/2+i\varepsilon,\quad \delta=\kappa_f q-\boldsymbol{\kappa}_f(\mathbf{s}-\boldsymbol{\kappa}_f)+i\varepsilon,\quad \varepsilon\to+0\ .\end{aligned} \tag{A8}$$

Explicit formulas for the evaluation of the cross section are given in Ref. 6. Note that the singularities inherent in (A7) are most conveniently handled by means of appropriate coordinate transformations.[6]

[1] *Forward Electron Ejection in Ion-Atom Collisions*, Vol. 213 of *Lecture Notes in Physics*, edited by K.-O. Groeneveld, W. Meckbach, and I. A. Sellin (Springer, Berlin, 1984).
[2] C. Bottcher, Phys. Rev. Lett. **48**, 85 (1982).
[3] R. Shakeshaft and L. Spruch, Phys. Rev. Lett. **41**, 1037 (1978).
[4] V. H. Ponce, J. Phys. B **14**, 3463 (1981).
[5] C. R. Garibotti and J. E. Miraglia, J. Phys. B **14**, 863 (1981).
[6] D. H. Jakubassa-Amundsen, J. Phys. B **16**, 1767 (1983).
[7] D. S. F. Crothers and J. F. McCann, J. Phys. B **20**, L19 (1987).
[8] W. Meckbach, I. B. Nemirovsky, and C. R. Garibotti, Phys. Rev. A **24**, 1793 (1981).
[9] P. Dahl, J. Phys. B **18**, 1181 (1985).
[10] S. D. Berry, G. A. Glass, I. A. Sellin, K.-O. Groeneveld, D. Hofmann, L. H. Andersen, M. Breinig, S. B. Elston, P. Engar, M. M. Schauer, N. Stolterfoht, H. Schmidt-Böcking, G. Nolte, and G. Schiwietz, Phys. Rev. A **31**, 1392 (1985).
[11] L. H. Andersen, K. E. Jensen, and H. Knudsen, J. Phys. B **19**, L161 (1986).
[12] H. Knudsen, L. H. Andersen, and K. E. Jensen, J. Phys. B **19**, 3341 (1986).
[13] L. Gulyás, Gy. Szabó, D. Berényi, Á. Kövér, K.-O. Groeneveld, D. Hofmann, and M. Burkhard, Phys. Rev. A **34**, 2751 (1986).
[14] D. Berényi (private communication).
[15] J. Macek, J. E. Potter, M. M. Duncan, M. G. Menendez, M. W. Lucas, and W. Steckelmacher, Phys. Rev. Lett. **46**, 1571 (1981).
[16] M. R. C. McDowell, Proc. R. Soc. London, Ser. A **264**, 277 (1961).
[17] J. S. Briggs, J. Phys. B **10**, 3075 (1977).
[18] D. H. Jakubassa-Amundsen, J. Phys. B **20**, 325 (1987).
[19] L. Sarkadi, J. Bossler, R. Hippler, and H. O. Lutz, Phys. Rev. Lett. **53**, 1551 (1984).
[20] R. Schramm, W. Oswald, H.-D. Betz, E. Szmola, and R. Schuch, *Abstracts of the Fifteenth International Conference on the Physis of Electronic and Atomic Collisions, Brighton, United Kingdom, 1987*, edited by J. Geddes, H. B. Gilbody, A. E. Kingston, C. J. Latimer, and H. R. J. Walters (Queens University, Belfast, 1987), p. 603; (to be published).
[21] M. W. Lucas, W. Steckelmacher, J. Macek, and J. E. Potter, J. Phys. B **13**, 4833 (1980).
[22] J. Burgdörfer, Phys. Rev. A **33**, 1578 (1986).
[23] L. J. Dubé and A. Salin, J. Phys B **20**, L499 (1987).
[24] A. Salin, J. Phys. B **2**, 631 (1969).
[25] J. E. Miraglia and V. H. Ponce, J. Phys. B **13**, 1195 (1980).
[26] D. H. Jakubassa-Amundsen, Ref. 1, p. 17.
[27] J. Burgdörfer, Phys. Rev. Lett. **51**, 374 (1983).
[28] G. Schiwietz (private communication); G. Schiwietz, D. Schneider, and J. Tanis, Phys. Rev. Lett. **59**, 1561 (1987).